REVISTA INVESTIGACIONES Y APLICACIONES NUCLEARES

SERVICIO GEOLÓGICO COLOMBIANO

Estimation of radioactive activity by gamma spectroscopy

Estimación de actividad radiactiva por espectroscopía gamma

Alejandro Restrepo[1] and Juan Sebastián Ramírez[1]

Revista Investigaciones y Aplicaciones Nucleares, 7, 2023
Received: August 12, 2022
Accepted: December 19, 2022
Published online: Frebruary 15, 2023
Doi: https://doi.org/10.32685/2590-7468/invapnuclear.7.2023.667

This work is licensed under a Creative Commons Attribution 4.0 International License

Citation: A. Restrepo and J. S. Ramírez, "Estimation of radioactive activity by gamma spectroscopy", *Revista Investigaciones y Aplicaciones Nucleares*, num. 7, 2023. https://doi.org/10.32685/2590-7468/invapnuclear.7.2023.667

Abstract

Radioactive sources of isotopes ^{22}Na, ^{137}Cs, ^{60}Co, ^{133}Ba and decay chains of Th and U are analyzed by means of gamma spectroscopy. The instrument used, a cylindrical NaI(Tl) scintillator from Mirion Technologies (Canberra) with dimensions of 2×2, is characterized by its calibration and absolute efficiency. The peak energies of the gamma spectra obtained are identified and related to corresponding isotopes and matter-radiation interactions according to nuclear and atomic databases. From these data, spectroscopic methods are implemented to compute radioactive activities for each source.

Keywords: Gamma spectroscopy, decay chain, radioactive activity, absolute efficiency.

Resumen

Fuentes radiactivas de los isótopos de ^{22}Na, ^{137}Cs, ^{60}Co, ^{133}Ba y las cadenas de decaimiento de Th y U son analizadas por medio de espectroscopía gamma. El instrumento usado; un centelleador cilíndrico de NaI(Tl) de Mirion Technologies (Canberra) con dimensiones 2×2 se caracteriza mediante su calibración y eficiencia absoluta. Los máximos de energías en los espectros gamma obtenidos son identificados y relacionados con sus isótopos correspondientes y las interacciones radiación-materia de acuerdo con bases de datos de estructura nuclear y atómica. A partir de estos datos, se implementan métodos espectroscópicos para calcular las actividades radiactivas de cada fuente.

Palabras clave: Espectroscopía gamma, cadena de decaimiento, actividad radiactiva, eficiencia absoluta.

[1] Instituto de Física, Universidad de Antioquia, Medellín, Colombia.
Corresponding author: Alejandro Restrepo, alejandro.restrepo19@udea.edu.co

1. Introduction

Atomic nuclei are susceptible to electromagnetic interactions in a similar way to how electrons are in larger atomic and molecular structures. Nuclei can absorb and emit photons of specific energies, which allows us to learn a great amount of information about their structure and identify certain isotopes in a given sample because, in the same way, there is a unique spectrum for every electronic configuration, every nuclear species has its own distinctive spectrum as well [3, 5]. Gamma spectroscopy focuses on the detection and measurement of such radiation emitted by atomic nuclei [1,2], even though signals from atomic electronic transitions and matter-radiation interactions are ubiquitous and end up being detected along with nuclear γ-rays. Another aspect to consider is that only gamma-emitting samples can be objects of spectroscopic analysis, so these must be naturally radioactive or artificially activated by specific techniques, such as neutron activation analysis (NAA), light nuclei bombarding activation, and high intensity γ-ray irradiation [6].

Due to these characteristics, gamma spectroscopy is applied to determine the presence and concentration of particular isotopes in radioactive sources. Its most common use is in analytical processes in which the samples have an intrinsic cultural, archaeological, academic or economical value and must not be destroyed chemically or by any means during its analysis. Additionally, for samples of sufficiently large dimensions for which not only the surface constitution but also the whole volume composition must be determined, gamma spectroscopy is a good option [7-9]. These techniques are used in the fields of geology, archaeology, medicine, nuclear forensics and industry [4], [7], [10].

Prior to any application, each isotope must be associated with a spectrum, so in this work, a group of four synthetic samples and two decay chains of naturally occurring radioactive elements were analyzed. The observed peaks were associated with γ-ray nuclei emissions of the highest absolute intensity with the assistance of nuclear structure databases [11-13] and similar references [14,15]. Subsequently, spectroscopy techniques are implemented to determine their corresponding radioactive activities.

The main purpose of this article is to show in detail how to perform a gamma spectroscopy analysis from the fundamental aspects of calibration, the efficiency of the instrument, expected spectra, the identification of radiation-matter interactions and activity estimation by elementary techniques as well as presenting some aspects to improve and perspectives to focus on the future. This article is presented as a more detailed and concise compilation of the methodologies to be implemented in a gamma spectroscopy exercise, which has been discussed in several references [3,4,5,16] but in a very scattered way and lacking many details in terms of the calculations and analyses. It is noteworthy that the explicit use of databases and the analysis presented allow this article to be a good pedagogical guide for beginners by providing tools that support and enhance their learning in this important experimental area.

2. Experimental setup and procedure

The instrument used was a cylindrical sodium iodide scintillator doped with thallium NaI(Tl) with dimensions of 2×2 (two inches in height and diameter) produced by the manufacturer Mirion Technologies (Canberra BNLS), which included the photomultiplier and amplifier [17]. This was located in a lead shield and connected to a computer that processed the measurements using the GENIE™ 2000 system. Photographs of the experimental setup are shown in Fig. 1.

The calibration process was performed to correctly identify the spectra, and the calculation of the instrument's efficiency was required for the estimation of the radioactive activity of the samples. For the calibration, it was required to associate energies E with channels c of the instrument such that they were able to be input into a cubic polynomial of the form

$$E = b + a_1 c + a_2 c^2 + a_3 c^3 \tag{1}$$

The known spectra of ^{137}Cs, ^{133}Ba and ^{60}Co were used for the energy-channel association. By a process of fitting, the resulting coefficients were

$$\begin{aligned} b &= 0.1 \pm 2.6 \\ a_1 &= 2.074 \pm 0.055 \\ a_2 &= (1.27 \pm 0.26) \times 10^{-3} \\ a_3 &= (-1.31 \pm 0.31) \times 10^{-6} \end{aligned} \tag{2}$$

Figure 1. a) Scintillator, lead shielding and sample mounting. b) Experimental setup for measurement

A first-degree polynomial may suffice for the calibration, as shown by the magnitudes of the parameters; however, we selected the three parameters to have a positive value of b and more refined energy-channel associations. A value of $R^2 = 0.99981$ was obtained. The calibration plot is shown in Figure 2.

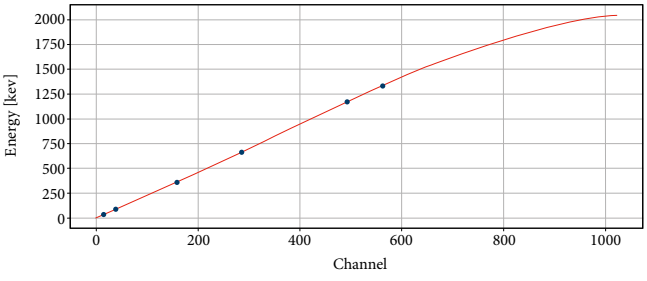

Figure 2. Channel vs. energy and calibration fit according to equation 2

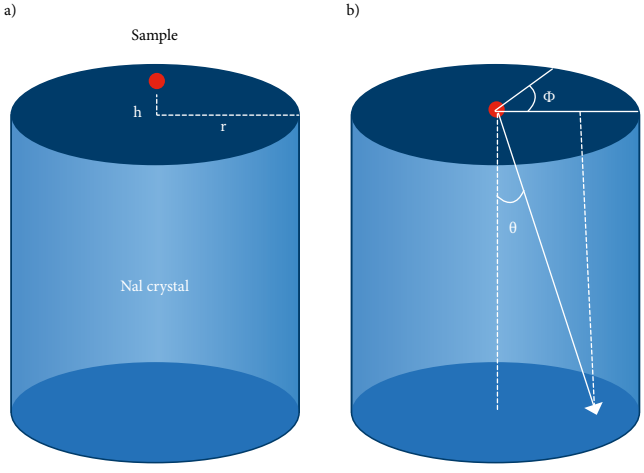

Figure 3. a) Samples and detector positioning. b). Coordinate system for $\bar{d}$ calculation

Figure 3 shows the positioning used for the samples with respect to the crystal with the variables $h = 0$ and $r = 1'' = 2.54$ cm. The sources were considered point sources for the following detector efficiency treatment.

The absolute efficiency ε was defined as the ratio between the quanta of radiation detected and those emitted by a sample. This had two contributions: one came from a factor associated with the extension and geometric shape of the instrument, and the other came from the probability that once the quantum of energy entered the sensitive volume of the instrument, it was effectively detected [3,18–20]. They were denoted as the geometric factor G and intrinsic efficiency ε_I, respectively. Then,

$$\varepsilon = G \times \varepsilon_I \tag{3}$$

The geometric factor was given by

$$G = \frac{\Omega}{4\pi} \tag{4}$$

where Ω is the solid angle subtended by the detector with respect to the sample. In this case, the sources were considered point sources, and due to the cylindrical shape of the detector, the solid angle was [20].

$$\Omega = 2\pi \left[1 - cos\left(arctan\left(\frac{r}{h}\right)\right)\right] \approx 2\pi \tag{5}$$

After applying the condition $h \to 0$, $G \approx 1/2$.

The intrinsic efficiency ε_I in turn had two contributions: one came from the probability I that a quantum of energy was transmitted to the NaI crystal by passing through the aluminum coating that isolated it from nonionizing radiation (see Figure 1) and the other came from the probability M that this quantum interacted with the sensible volume of the crystal and was therefore measured. In the case of electromagnetic radiation, these quantities have the form [18]

$$\begin{aligned} I &= \mathrm{e}^{-\mu_{Al}(E)\,d_1} \\ M &= 1-\mathrm{e}^{-\mu_{NaI}(E)\,d_2} \end{aligned} \tag{6}$$

where d_1 and d_2 are the paths that the photons travel and $\mu(E)$ are the linear attenuation coefficients that depend on the energy of the photon in question. For the energies of interest, $\mu_{Al}(E)$ has small values on the order of 10^{-1} according to the National Institute of Standards and Technology (NIST) [21] database. In addition, the coating of the crystal was of a negligible thickness of $d_1 = 2.5$ mm. Therefore, the approximation $I \approx 1$ was considered.

For d_2, we calculated the mean value of the distances from the center of one of the circular faces to the points of the other two surfaces of the cylinder, that is, all the possible paths of the γ-rays through the detector's crystal. The coordinate system for this calculation is shown in Figure 3.

Mathematically, this expression is

$$d_2 = \overline{d} = \frac{\int_0^{2\pi}\int_0^{\pi/2} d(\theta,\phi)\,d\theta\,d\phi}{\pi^2} \approx 1.53'' \pm 0.12'' = 3.89 \pm 0.31 \text{ cm} \tag{7}$$

where

$$d(\theta,\phi) = \begin{cases} 2\,sec\,(\theta), & 0 \le \theta \le \arctan(0.5) \\ csc\,\theta, & \arctan(0.5) < \theta < \pi/2 \end{cases}$$

is the distance dependent on the surface of the cylinder on which it is integrated. The uncertainty was computed using error propagation considering the diameter and height as $2.0'' \pm 0.1''$. This calculation was equivalent to replacing the cylindrical shape of the crystal by a virtual hemisphere of radius d.

Then, the following was obtained

$$\varepsilon = \frac{1-\mathrm{e}^{-3.89 \times \mu_{NaI}(E)}}{2} \tag{8}$$

where the $\mu_{NaI}(E)$ function with units of cm^{-1} was evaluated for particular energies [18].

The efficiency plot for a certain range of energies of interest is shown in Figure 4. Due to the complex dependence of μ_{NaI} on E, these points were fit to a negative exponential whose functional form is shown in the same figure. The fit resulted in a value of $R^2 = 0.99074$.

The samples used are shown in Figure 5. The thorium sample came from a thoriated tungsten electrode at 1-2%, which initially had a length of ≈15 cm and was prepared in ≈1 cm pieces such that it approximated a point source. It was considered to be composed of the isotope ^{232}Th and its associated decay chain because it is the Th isotope of largest abundance in nature, a claim verified by the obtained spectrum. Similarly, the uranium sample was considered to be composed of the isotope ^{238}U and its associated decay chain. Samples of ^{22}Na, ^{137}Cs, ^{60}Co, and ^{133}Ba were artificially produced as standards for the calibration of the gamma spectroscopy detectors. The measurements were collected for 10 minutes, except for the thorium sample, which required a time of 30 minutes due to its low activity. The same time intervals were adopted for the measurement of background radiation, that is, 30 minutes for thorium and 10 minutes for the others.

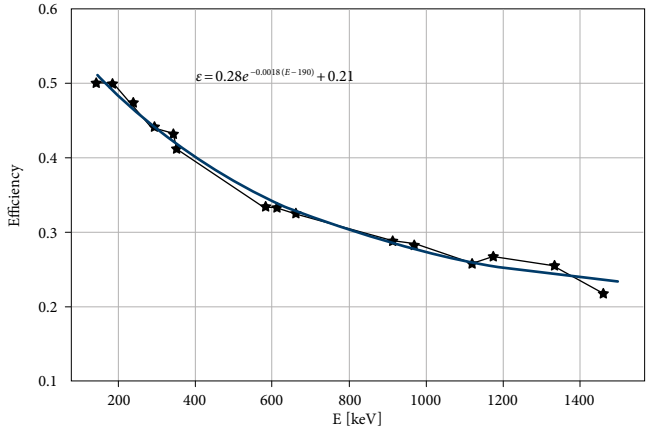

Figure 4. Absolute efficiency of the instrument used and experimental configuration

3. Results and analysis

The spectra obtained for ^{22}Na, ^{137}Cs, ^{60}Co, and ^{133}Ba are shown in Figures 7 to 10 with their respective diagrams of decay. The spectra of ^{232}Th and ^{238}U are shown in Figures 11 and 12 with their associated decay chains. Net counts were smoothed by a convolution known as the moving average. The maxima of

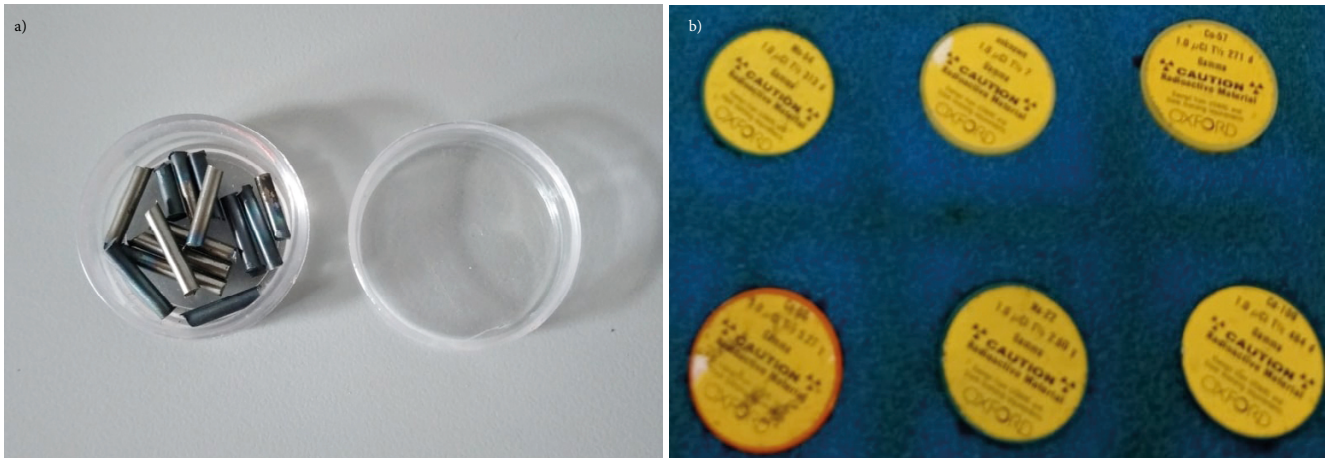

Figure 5. a) Thorium sample. b). Samples of ^{22}Na, ^{137}Cs, ^{60}Co and ^{133}Ba

the spectra were identified based on nuclear structure databases [11-13] and similar articles [14], [15], [22].

In addition to observing the emissions of gamma rays from the de-excitation of nuclei after radioactive decay, X-ray spectra were also observed from atomic orbital rearrangements and radiation-matter interactions. The latter was observed as positron electron annihilation ($e^+ e^- \rightarrow 2\gamma$) at 510.99895 keV, the Compton effect, X-rays from lead shielding of 72-87 keV [23], [24] and backscattering at approximately 0.2-0.25 MeV [3] due to the same shielding, which is indicated by shaded areas under the measured spectrum.

For the calculation of the activities, two methods were implemented to obtain the net counts of the distinguishable peaks of the measured spectra. These are called the straight-line tangent method and reflection method. The first was applied in isolated spikes on the background signal from the superposition of continuous Compton and backscattering. An excellent example is the ^{214}Bi peak at 609.320 keV of the spectrum of uranium. This method consisted of considering a tangent line in the minimum values of the peak such that it was taken as the signal of background and calculating the net counts of the peak by subtracting those given by such line [3]. This is demonstrated graphically in Figure 6.

On the other hand, the reflection method was applied on indistinguishable peaks, that is, those in which the widths at half height were overlapping. An additional condition was that the overlapping peaks did not overlap with other spectrum peaks to the right or left. Examples of cases where this method is applicable are those of ^{60}Co and for uranium those of ^{214}Pb at 351.932 keV and ^{226}Ra at 186.211 keV. Then, the counts from the maximum to the minimum nonoverlapping peaks were multiplied by two to take into account the indistinguishable part of the signal [25]. If the peaks had a signal background, it was also necessary to apply the tangent method simultaneously. This is shown in Figure 6.

These methods were implemented for 10 peaks of the spectra obtained. Once the number of counts was obtained, the activity was calculated using the following equation [18]:

$$A = \frac{N}{TI\gamma\varepsilon} \tag{9}$$

where N is the number of counts, T is the measurement time, $I\gamma$ is the absolute intensity of a given γ-ray obtained from [11], and ε is the absolute efficiency of the detector obtained from Equation 8.

The results for these methods are shown in Table 1. Calculation of the uncertainties was performed considering the double of the standard deviation of each peak using Poisson distributions [3]. The procedure for ^{22}Na required a division by 2 of the counts N because the 510.998 keV peak corresponded to the process $e^+e^= \rightarrow 2\gamma$, where every two gamma rays detected corresponds to a single nuclear decay.

Table 1. Estimated radioactive activities of the identi fied isotopes

Isotope	Activity [Bq]
^{22}Na	4.2 ± 0.5
^{137}Cs	14436 ± 19
^{60}Co	89 ± 2
^{133}Ba	1509 ± 5
Thorium decay chain isotopes	
^{228}Ac	41 ± 4
^{212}Pb	28 ± 2
^{208}Tl	8.3 ± 0.8
Uranium decay chain isotopes	
^{226}Ra	18442 ± 80
^{214}Pb	9043 ± 17
^{214}Bi	6825 ± 20

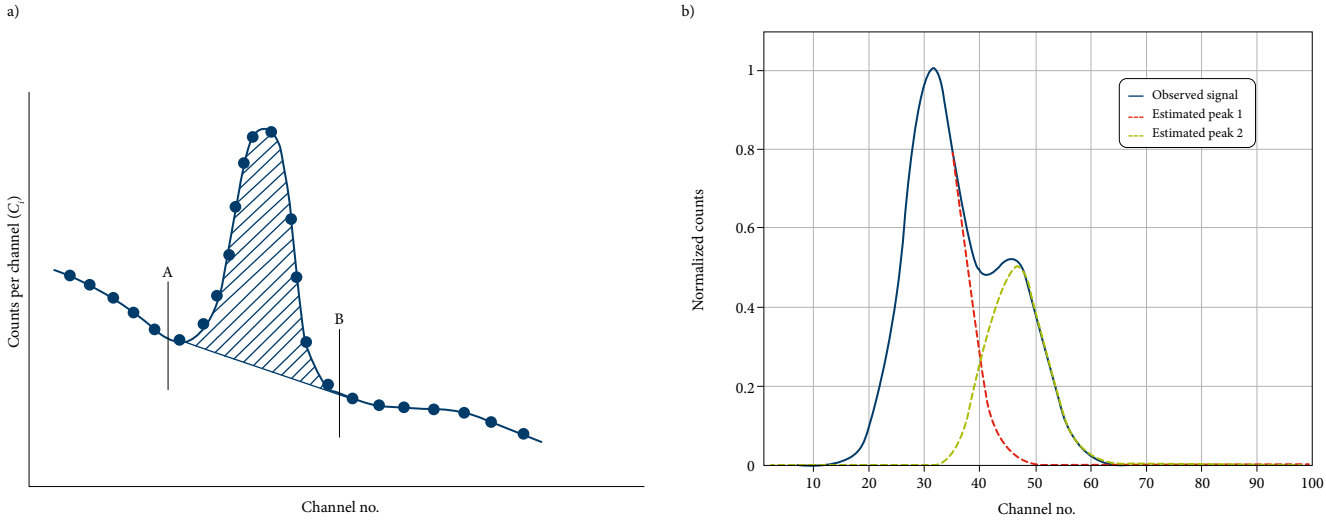

Figure 6. a) Tangent method [3]. b) Reflection method [25]

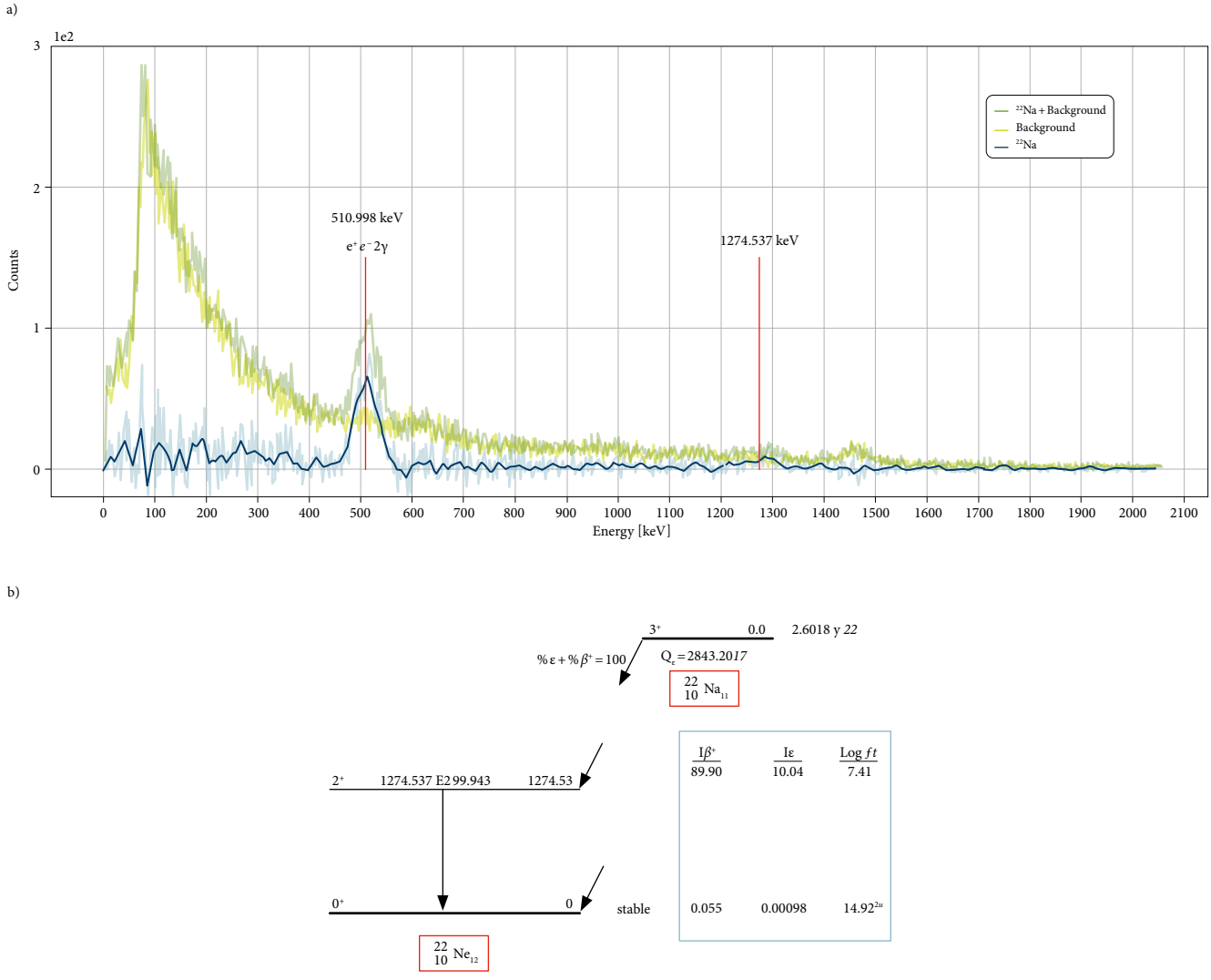

Figure 7. a) ^{22}Na spectrum. b) Decay diagram
Souce: Taken from NNDC [11].

a)

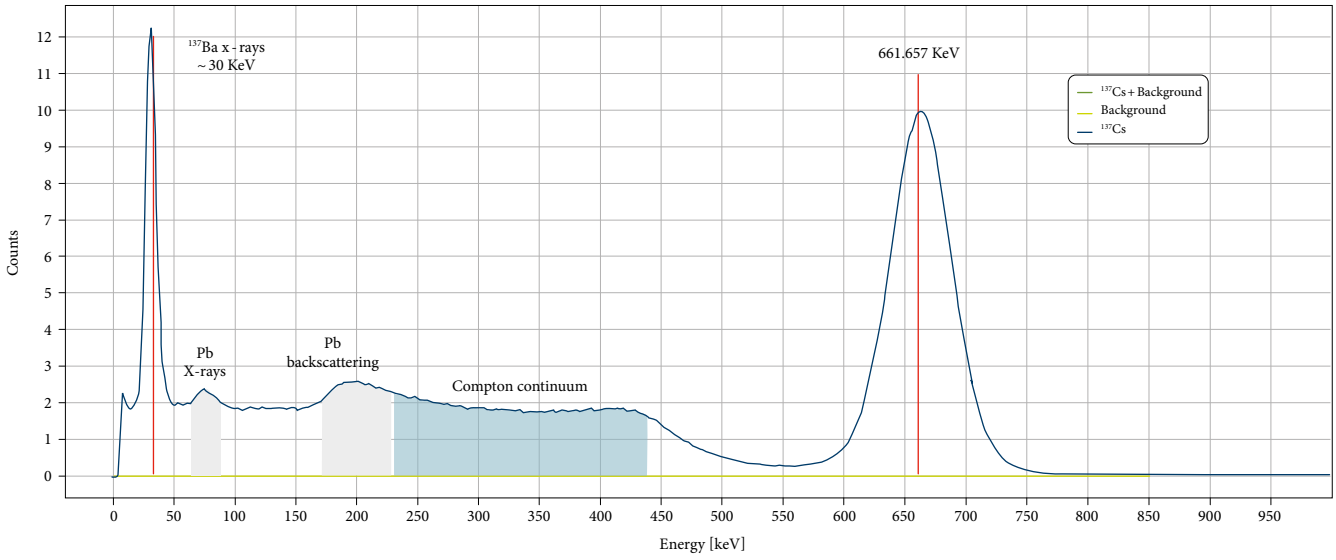

b)

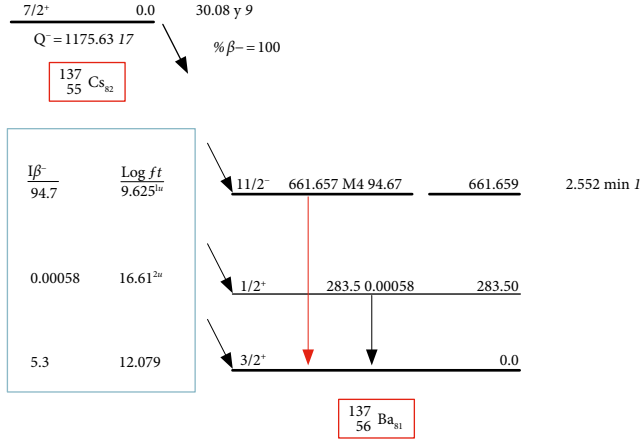

Figure 8. Upper: ^{137}Cs spectrum. Bottom: Decay diagram. Taken from NNDC [11]

a)

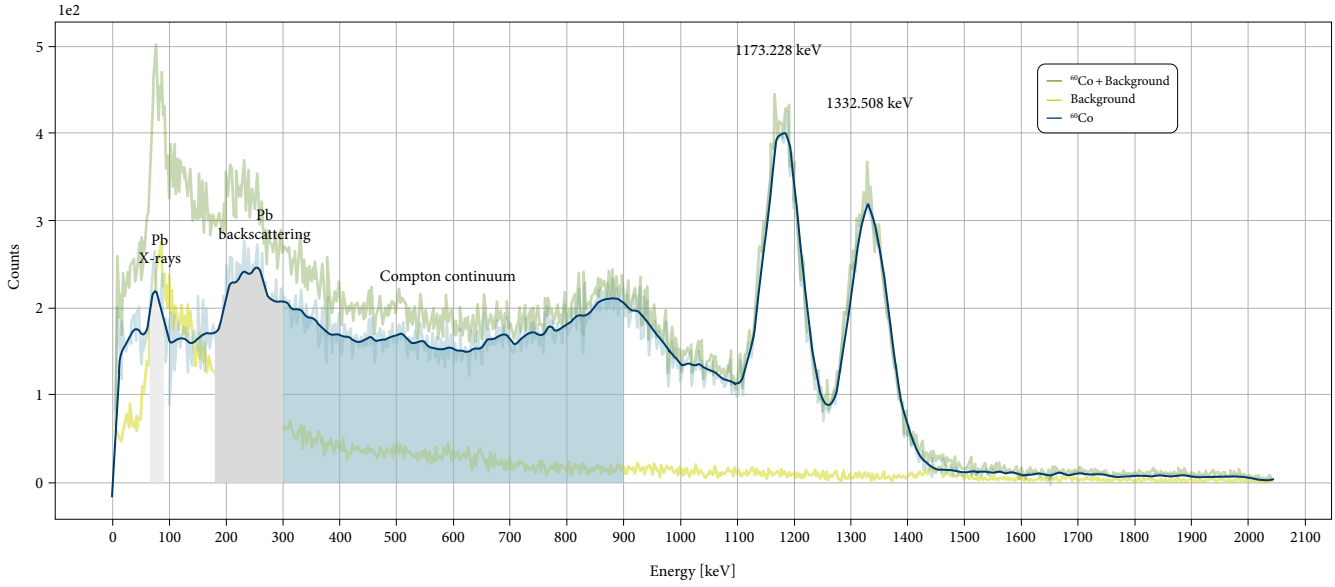

b)

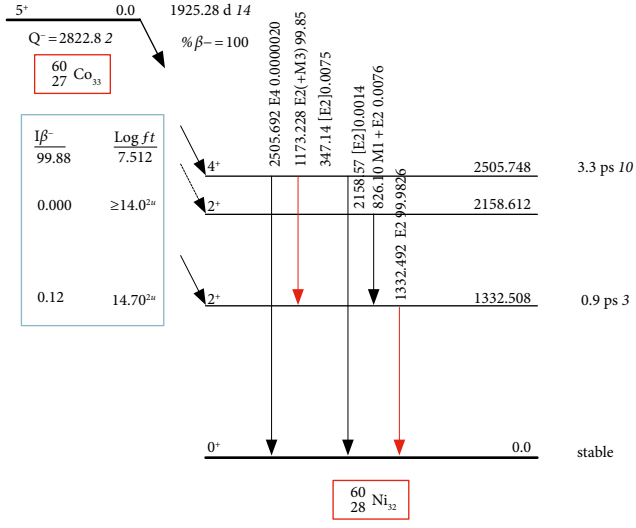

Figure 9. a) ^{60}Co spectrum. b) Decay diagram
Source: Taken from NNDC [11].

a)

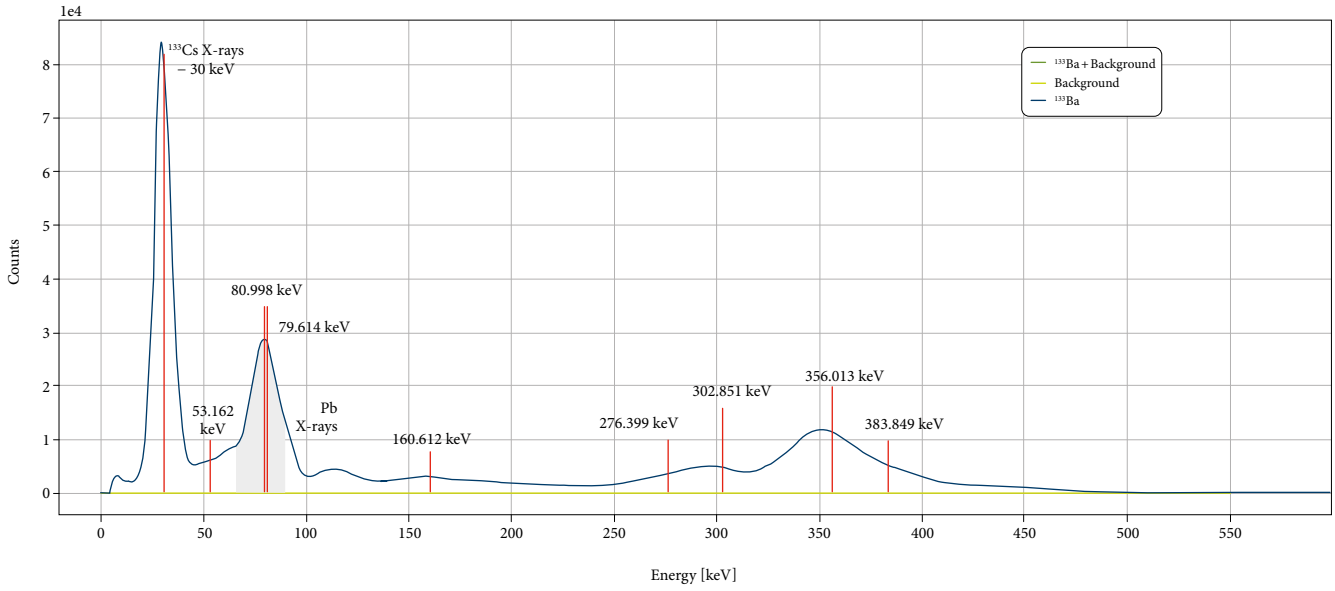

b)

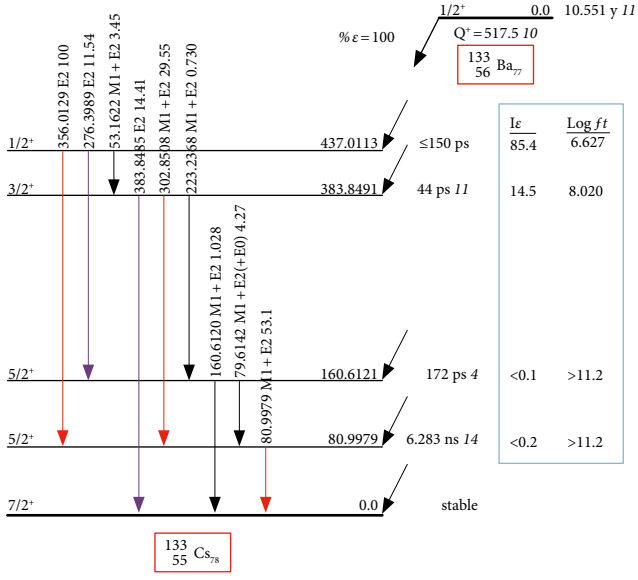

Figure 10. a) ^{133}Ba spectrum. b) Decay diagram. Taken from NNDC [11]

a)

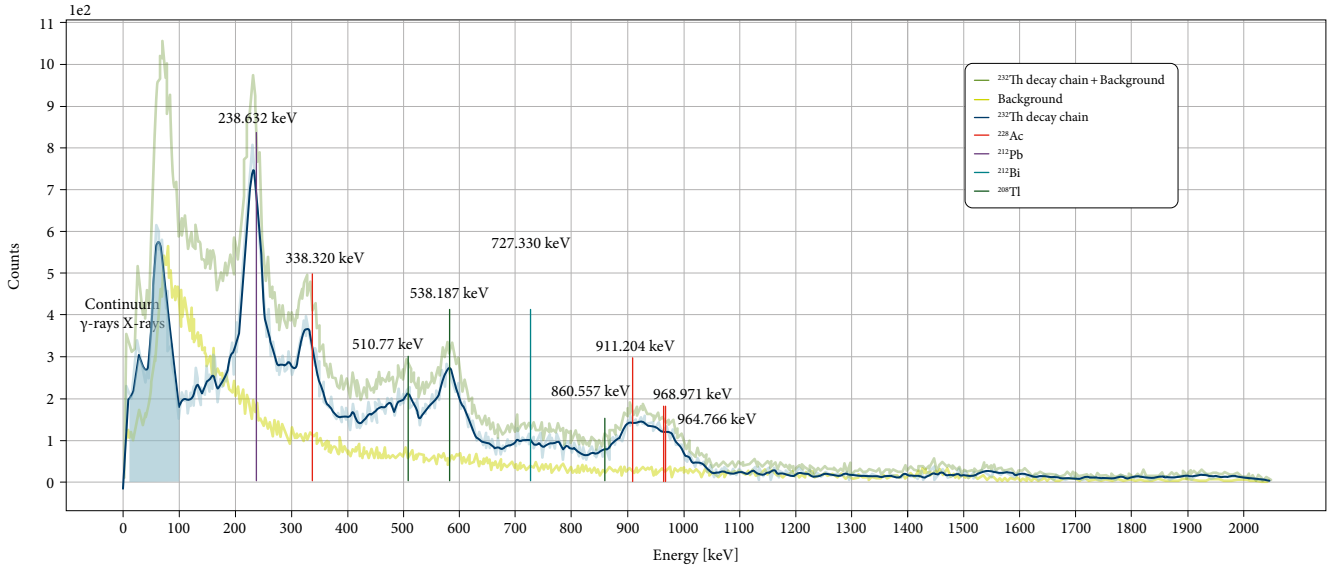

b)

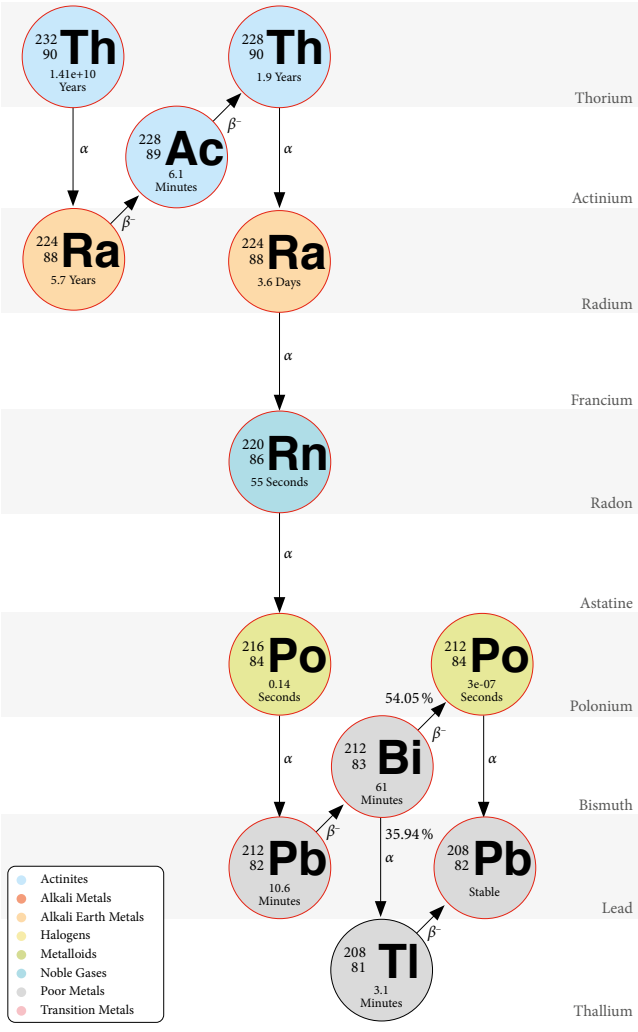

Figure 11. a) ^{232}Th decay chain spectrum. b) Decay chain. The most likely decay is shown in red
Source: Taken from Wikimedia Commons with license Creative Commons Attribution-Share Alike 3.0 Unported [26].

a)

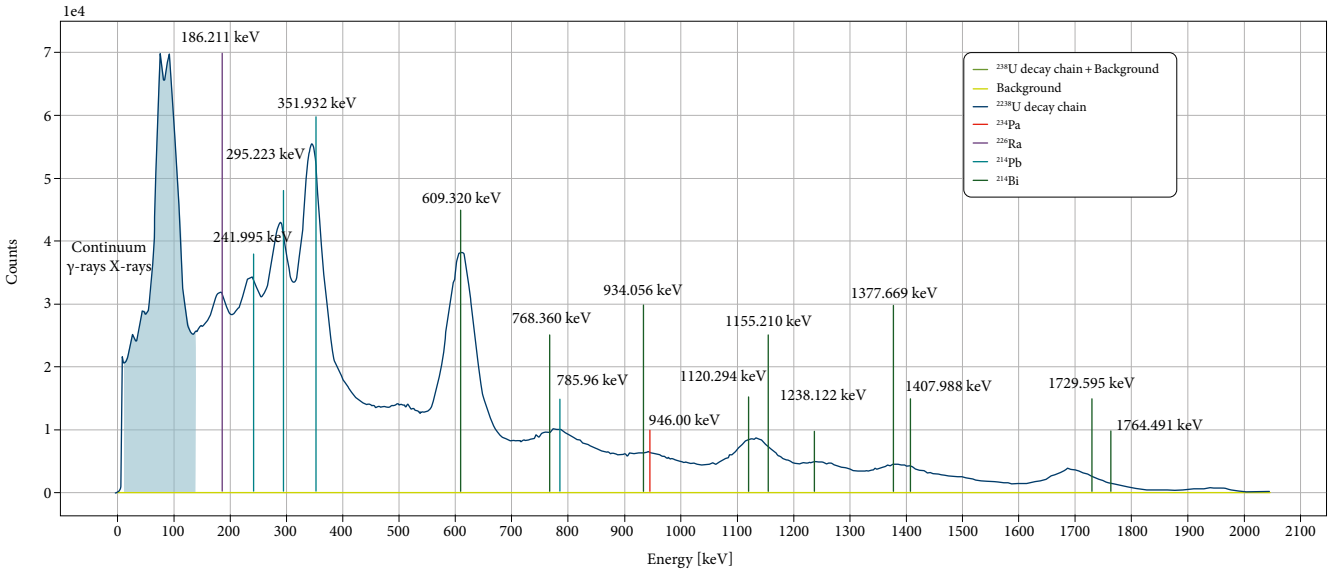

b)

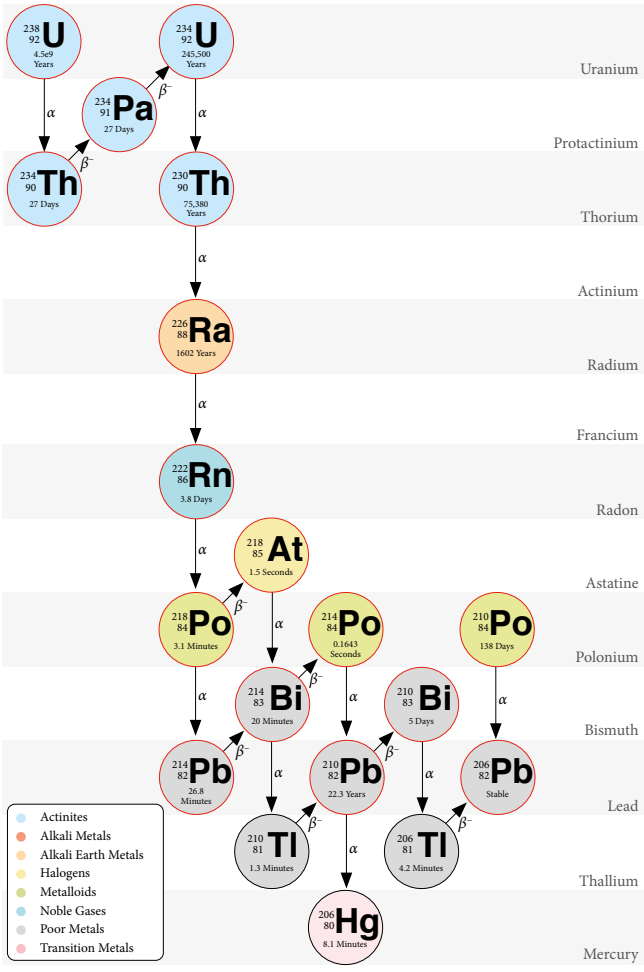

Figure 12. a) ^{238}U decay chain spectrum. b) Decay chain. The most likely decay is shown in red
Source: Taken from Wikimedia Commons with license Creative Commons Attribution-Share Alike 4.0 International [27].

4. Conclusions

The most significant electromagnetic energies of each sample were recognized according to nuclear structure databases, and their corresponding emitting isotopes were identified, which allowed the estimation of the concentrations of each isotope. In the spectra, apart from the gamma emissions, it is possible to observe other phenomena related to transitions in electronic orbitals and

radiation-matter interactions, such as the Compton effect, positron-electron annihilation and backscattering with the shielding of lead.

The characterization of the instrument in terms of calibration and efficiency calculation allowed the identification of the most significant energies and estimation of the radioactive activities of the identified isotopes in conjunction with the spectroscopic techniques of the tangent and reflection method. The methodology proposed can be generalized for similar experimental setups and analyses of gamma spectroscopy measurements.

These results would be improved with longer times of data collection on the order of hours and with an instrument of better resolution, such as high-purity germanium detectors (HPGe). However, this type of detector has a much lower efficiency, which requires even longer counting times. A more rigorous treatment of the spectra obtained for the determination of activities, possibly with the implementation of specialized software, would also improve the results. Some perspectives remain as well, such as the efficiency calculation of nonpunctual samples where the same procedure must be followed but with changes in the mathematical expressions of the solid angle and mean distance of gamma ray paths. Another aspect to focus on is the estimation of the concentration of a given isotope in samples subjected to this experimental procedure. The general aspects of the methodology can be followed and reproduced to improve the calculations for different radioactive samples and instruments.

5. Acknowledgements

We thank Professor Gloria María Díaz Londoño of the Universidad Nacional de Colombia, Medellin, for advising us and providing us with the necessary equipment for this project. We thank the professors Oscar Luis Arnache Olmos and Alejandro Vélez Zea for helping us contact her and for their guidance during the development of the project.

References

[1] K. S. Krane, *Introductory nuclear physics*. New York, NY: Wiley, 1988.

[2] S. G. Prussin, *Nuclear physics for applications: a model approach*. Wiley-VCH, 2007.

[3] G. F. Knoll, *Radiation detection and measurement*, 2nd ed. Wiley New York, 1989.

[4] N. Tsoulfanidis, *Measurement and detection of radiation*, 4th edition. Boca Raton, FL: CRC Press, 2015.

[5] S. Tavernier, *Experimental Techniques in Nuclear and Particle Physics*. Berlin, Germany: Springer, 2010. https://doi.org/10.1007/978-3-642-00829-0

[6] E. V. Sayre, "Methods and Applications of Activation Analysis", *Annual Review of Nuclear Science*, vol. 13, no. 1, pp. 145-162, 1963, https://doi.org/10.1146/annurev.ns.13.120163.001045

[7] M. Moussa, "Gamma-ray spectrometry: a new tool for exploring archaeological sites; a case study from East Sinai, Egypt", *Journal of Applied Geophysics*, vol. 48, no. 3, pp. 137-142, 2001, https://doi.org/10.1016/S0926-9851(01)00077-5

[8] J. Sanjurjo-Sánchez, C. Arce Chamorro, C. Alves, J. C. Sánchez-Pardo, R. Blanco-Rotea, and J. M. Costa-García, "Using in situ gamma ray spectrometry (GRS) exploration of buried archaeological structures: A case study from NW Spain", *Journal of Cultural Heritage*, vol. 34, pp. 247-254, 2018, https://doi.org/10.1016/j.culher.2018.05.004

[9] P. B. Siegel, "Gamma spectroscopy of environmental samples", *American Journal of Physics*, vol. 81, no. 5, pp. 381-388, 2013, https://doi.org/10.1119/1.4793595

[10] E. B. Norman, "Nuclear Forensics using Gamma-ray Spectroscopy", *EPJ Web Conf.*, vol. 123, p. 04001, 2016, https://doi.org/10.1051/epjconf/201612304001

[11] *National Nuclear Data Center*. https://www.nndc.bnl.gov/

[12] *International Atomic Energy Agency Nuclear Data Services*. https://www-nds.iaea.org/

[13] *Laboratoire National Henri Becquerel Atomic and Nuclear data*. http://www.lnhb.fr/nuclear-data/module-lara/

[14] D. M. M. Olivares, E. S. Koch, M. V. M. Guevara, and F. G. Velasco, "Determination of uranium and thorium using gamma spectrometry: a pilot study", *Journal of Physics: Conference Series*, vol. 975, p. 012035, Mar. 2018, https://doi.org/10.1088/1742-6596/975/1/012035

[15] M. Długosz-Lisiecka, "Comparison of two spectrometric counting modes for fast analysis of selected radionuclides activity", *Journal of Radioanalytical and Nuclear Chemistry*, vol. 309, pp. 941-945, 2016, https://doi.org/10.1007/s10967-015-4688-y

[16] G. Gilmore, "Practical Gamma-Ray Spectrometry", 2nd Edition, Wiley-VCH Verlag, Wenheim, Germany, 2008.

[17] *02 Scintillation Detectors*. Mirion Technologies (Canberra) Inc., 2017. [Online]. https://mirion.s3.amazonaws.com/cms4_mirion/files/pdf/spec-sheets/csp0232_802_super_spec_2.pdf?1557861234

[18] A. Kadum, and B. Dahmani, "Efficiency calculation of NaI(Tl) 2 × 2 well-shaped detector", *Instruments and Experimental Techniques*, vol. 58, pp. 429-434, 2015, https://doi.org/10.1134/S0020441215030070

[19] I. Mouhti, A. Elanique, M. Y. Messous, B. Belhorma, and A. Benahmed, "Validation of a NaI(Tl) and LaBr3(Ce) detector's models via measurements and Monte Carlo simulations", *Journal of Radiation Research and Applied Sciences*, vol. 11, no. 4, pp. 335-339, 2018, https://doi.org/10.1016/j.jrras.2018.06.003

[20] S. Ahmadi, S. Ashrafi, and F. Yazdansetad, "A method to calculate the gamma ray detection efficiency of a cylindrical NaI (Tl) crystal", *Journal of Instrumentation*, vol. 13, no. 5, pp. P05019-P05019, May 2018, https://doi.org/10.1088/1748-0221/13/05/p05019

[21] *X-Ray Mass Attenuation Coefficients*. https://physics.nist.gov/PhysRefData/XrayMassCoef/tab3.html

[22] S. Sadasivan, and V. M. Raghunath, "Intensities of gamma rays in the 232Th decay chain", *Nuclear Instruments and Methods in Physics Research*, vol. 196, no. 2, pp. 561-563, 1982, https://doi.org/10.1016/0029-554X(82)90153-7

[23] *X-ray Transition Energies Database Main Page*. https://physics.nist.gov/PhysRefData/XrayTrans/Html/search.html

[24] M. L. Smith, L. Bignell, D. Alexiev, L. Mo, and J. Harrison, "Evaluation of lead shielding for a gamma-spectroscopy system", *Nuclear Instruments and Methods in Physics Research Section A: Accelerators, Spectrometers, Detectors and Associated Equipment*, vol. 589, no. 2, pp. 275-279, 2008, https://doi.org/10.1016/j.nima.2008.02.050

[25] T. C. O'Haver, *A Pragmatic Introduction to Signal Processing*. Kindle Direct Publishing, 2022.

[26] https://commons.wikimedia.org/wiki/File:Decay_Chain_of_Thorium.svg

[27] https://commons.wikimedia.org/wiki/File:Decay_Chain_of_Uranium-238.svg